CTP:Phosphocholine Cytidylyltransferase Binds Anionic Phospholipid Vesicles in a Cross-Bridging Mode†

Svetla G. Taneva,[‡,§] Philipus J. Patty,[§,||] Barbara J. Frisken,[||] and Rosemary B. Cornell*[,‡,⊥]

Department of Molecular Biology and Biochemistry, Department of Physics, and Department of Chemistry, Simon Fraser University, Burnaby, BC, Canada V5A 1S6

Received April 13, 2005; Revised Manuscript Received May 11, 2005

ABSTRACT: CTP:phosphocholine cytidylyltransferase (CCT) catalyzes the rate-limiting step in phosphatidylcholine (PC) synthesis, and its activity is regulated by reversible association with membranes, mediated by an amphipathic helical domain M. Here we describe a new feature of the CCTα isoform, vesicle tethering. We show, using dynamic light scattering and transmission electron microscopy, that dimers of CCTα can cross-bridge separate vesicles to promote vesicle aggregation. The vesicles contained either class I activators (anionic phospholipids) or the less potent class II activators, which favor nonlamellar phase formation. CCT increased the apparent hydrodynamic radius and polydispersity of anionic phospholipid vesicles even at low CCT concentrations corresponding to only one or two dimers per vesicle. Electron micrographs of negatively stained phosphatidylglycerol (PG) vesicles confirmed CCT-mediated vesicle aggregation. CCT conjugated to colloidal gold accumulated on the vesicle surfaces and in areas of vesicle−vesicle contact. PG vesicle aggregation required both the membrane-binding domain and the intact CCT dimer, suggesting binding of CCT to apposed membranes via the two M domains situated on opposite sides of the dimerization domain. In contrast to the effects on anionic phospholipid vesicles, CCT did not induce aggregation of PC vesicles containing the class II lipids, oleic acid, diacylglycerol, or phosphatidylethanolamine. The different behavior of the two lipid classes reflected differences in measured binding affinity, with only strongly binding phospholipid vesicles being susceptible to CCT-induced aggregation. Our findings suggest a new model for CCTα domain organization and membrane interaction, and a potential involvement of the enzyme in cellular events that implicate close apposition of membranes.

CCT[1] is an amphitropic protein. It interconverts between a soluble inactive form and a membrane-bound active form. Membrane binding and activation of CCT are regulated by changes in membrane lipid composition and the phosphorylation state of CCT (*1*). Studies in vitro (*2*−*5*) and in vivo (*5*−*9*) have identified two classes of lipids that promote membrane binding and activation of CCT. Class I lipids (anionic phospholipids) generate a negative electrostatic surface potential which attracts CCT to the membrane surface followed by hydrophobic interactions and insertion of CCT into the interfacial region of the outer monolayer of the bilayer (*2*, *4*, *5*). Class II lipids, such as diacylglycerols and unsaturated phosphatidylethanolamine, induce negative curvature strain, and binding of CCT to class II lipid membranes might relieve this curvature strain (*10*, *11*). Long chain fatty acids also promote CCT membrane binding, and share features of both class I and class II lipid activators. Direct and indirect binding measurements of the full enzyme or peptides comprising the membrane binding domain suggest that the binding affinity of CCT for anionic phospholipids exceeds that for fatty acids or class II lipids by more than 10-fold (*3*, *4*, *10*, *11*). In cells, CCT translocates to the nuclear envelope (*7*, *12*−*14*) or ER (*15*, *16*), in response to stimuli that accelerate PC synthesis. These cellular membranes contain both class I and II lipids (*17*, *18*).

CCT is a homodimer (*19*), and each subunit consists of three main functional domains. The N-terminal head (amino acids 1−236) contains the conserved catalytic domain (*20*) and, together with the domain preceding it (domain N), is responsible for subunit dimerization (*21*). The membrane-binding domain (domain M, residues ∼237−299) adopts an amphipathic helical structure upon membrane binding (*4*, *5*, *22*, *23*). The C-terminal serine- and proline-rich region (domain P) is highly phosphorylated (*24*), and its phospho-

† This work was supported by the Canadian Institutes for Health Research (Grant MT-12134 to R.B.C.) and NSERC of Canada (to B.J.F.).

* To whom correspondence should be addressed. Phone: (604) 291-3709. Fax: (604) 291-5583. E-mail: cornell@sfu.ca.

‡ Department of Molecular Biology and Biochemistry.

§ These authors contributed equally to this work.

|| Department of Physics.

⊥ Department of Chemistry.

[1] Abbreviations: CCT, α isoform of CTP:phosphocholine cytidylyltransferase; CCT236, fragment comprising residues 1−236 of rat CCTα; domain M peptide, synthetic peptide based on residues 237−293 of rat liver CCTα; DLS, dynamic light scattering; TEM, transmission electron microscopy; EDTA, ethylenediaminetetraacetic acid; CF, 5(6)-carboxyfluorescein; NBD-PE, *N*-(7-nitrobenz-2-oxa-1,3-diazol-4-yl)-1,2-dihexadecanoyl-*sn*-glycero-3-phosphoethanolamine; Rho-PE, lissamine rhodamine B 1,2-dihexadecanoyl-*sn*-glycero-3-phosphoethanolamine; DOG, 1,2-dioleoyl-*sn*-glycerol; DOPE, 1,2-dioleoyl-*sn*-glycero-3-phosphoethanolamine; PS, 1-palmitoyl-2-oleoyl-*sn*-glycero-3-phospho-L-serine; DTT, dithiothreitol; PC, egg phosphatidylcholine; PG, egg phosphatidylglycerol; OA, oleic acid; LUV, large unilamellar vesicle; SUV, small unilamellar vesicle; SLV, sucrose-loaded vesicle.

10.1021/bi050679p CCC: $30.25
Published on Web 06/11/2005

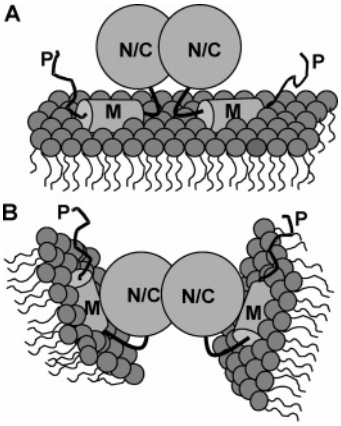

FIGURE 1: Two modes for CCT association with membranes. (A) CCT interacts with its two M domains partitioning into a single vesicle. (B) CCT cross-bridges two lipid bilayers through interactions of each domain M with separate vesicles. N/C represents the N-terminal and catalytic domains, M the membrane binding amphipathic helical domain, and P the C-terminal phosphorylation domain.

rylation decreases membrane affinity (*3*, *7*, *25*, *26*). A catalytic fragment of CCT lacking domains M and P (CCT236) did not translocate to membranes in response to oleic acid, and was constitutively active (*27*, *28*). These observations have generated a model for activation of CCT in which domain M is an inhibitor of the catalytic domain. The inhibition is relieved upon membrane binding of domain M (*27*, *28*). Models of CCT−membrane interaction have depicted an arrangement in which the two M domains of the CCT dimer engage the same membrane surface (*1*; Figure 1A).

In a previous study, we noted that addition of CCT to anionic phospholipid SUVs increased the turbidity of the suspensions (*23*). This observation suggested that CCT can induce the aggregation of vesicles via a CCT-mediated cross bridge in which the two M domains of the CCT dimer engage two separate vesicles (Figure 1B). To explore the cross-bridging model more rigorously, we used DLS and TEM to examine the effects of the full-length CCT, a domain M fragment, or an N-terminal fragment missing domains M and P on the size and aggregation state of LUVs containing class I or class II lipid activators. Both methods revealed that *only* the full-length CCT promotes the aggregation of *only* vesicles containing anionic phospholipids, in support of the cross-bridging model. CCT did not induce the aggregation of vesicles containing the more weakly activating class II lipids. The CCT fragments did not induce aggregation of any vesicles that were studied. These observations give rise to a new hypothesis for the organization of CCT domains involving the positioning of domain M on opposite poles of the catalytic dimer and suggest the potential for CCT to act as a vesicle tether.

EXPERIMENTAL PROCEDURES

Materials

Egg PC and PG were purchased from Northern Lipids Inc. (Vancouver, BC). DOPE and PS were from Avanti Polar Lipids. The purity of phospholipid stocks was confirmed by thin-layer chromatography, and the concentrations of the phospholipids were determined with a phosphorus assay (*29*). CTP, DTT, DEAE-Sepharose, CM-Sepharose, Blue Sepharose (fast flow), Triton X-100, and OA were from Sigma. CF was from Kodak, and NBD-PE and Rho-PE were from Molecular Probes.

Methods

Expression and Purification of CCT. The rat liver CCTα isoform and CCTα236 (encoding amino acids 1−236) were expressed by baculovirus infection of *Trichoplusia ni* cells and purified as described previously (*11*, *23*). The pure enzymes were stored in aliquots at −80 °C, and their concentrations were determined by quantitative amino acid analysis (Alberta Peptide Institute, Edmonton, AB). Both CCT preparations were homogeneously pure based on a Coomassie stain of SDS−PAGE samples.

Peptide Synthesis. A 57-mer peptide corresponding to residues 237−293 of rat liver CCTα was synthesized by K. Piotrowska at the University of British Columbia Peptide Service Laboratory (Vancouver, BC) as described previously (*23*). The concentration of an aqueous stock solution (∼1 mM) was determined by measuring the absorbance at 280 nm (ϵ = 6970 M^{-1} cm^{-1}).

Preparation of Large Unilamellar Vesicles (LUVs) and Vesicle Turbidity Assay. Lipid mixtures were prepared from chloroform stocks, dried by rotary evaporation, and placed under vacuum overnight to remove trace residual solvent. The lipid films were resuspended in prefiltered buffer A [10 mM Tris (pH 7.4), 1 mM EDTA, 150 mM NaCl, and 10 mM DTT] to a concentration of 0.4 mM. The suspensions were subjected to five freeze−thaw−vortex cycles to disrupt multilamellar structure, diluted to 0.1 mM, and extruded 14 times at a pressure of 200 psi through two polycarbonate membranes with a nominal pore diameter of 50 nm using an extruder (Lipex Biomembranes, Vancouver, BC). The final phospholipid concentrations were determined by the method of Bartlett (*29*). The LUVs were stored at 4 °C and were used within 3 days of preparation. To determine the ratio of CCT monomers to vesicle, we calculated the number of lipids per vesicle using the vesicle hydrodynamic radii determined by DLS (this study), a bilayer thickness of 4 nm (*30*), and a headgroup area of 0.68 nm^2 for PG, PC, and PS (*31*) and 0.28 nm^2 for OA. The latter represents the area per molecule in monomolecular layers of OA at the maximal surface pressure of ∼30 mN/m (*32*). By this calculation, LUVs of PG contain ∼60000 lipids/vesicle.

CCT-induced vesicle aggregation was assayed at 20 °C by measuring the increase in the apparent absorbance at 400 nm of LUV suspensions after addition of CCT (*23*).

CCT Activity Assay. Activity was measured in the presence of varying concentrations of LUVs as described previously (*3*). The concentration of CCT was 22 nM, and the other components were 20 mM Tris (pH 7.4), 10 mM DTT, 88 mM NaCl, 12 mM $MgCl_2$, 8 mM CTP, and 1.6 mM [^{3}H]-phosphocholine, with a specific activity of 10 mCi/mmol.

Membrane Binding Assay. Sucrose-loaded vesicles (SLVs) containing trace amounts of [^{3}H]DPPC were prepared in 20 mM Tris (pH 7.4), 170 mM sucrose, and 10 mM DTT, extruded through two 0.1 μm polycarbonate filters, and sedimented as described previously (*3*). CCT (0.8 μM) in buffer A was incubated with SLVs (0.05−1.2 mM lipid) in a total volume of 60 μL for 20 min at room temperature.

The membrane-bound CCT was separated from the free enzyme by centrifugation at 100000*g* for 30 min at 25 °C. The pellets contained greater than 90% of the lipid as determined from radioactivity. The quantity of CCT in the pellet and supernatant was determined by SDS−PAGE using a Tricine gel system. Gels were stained with SYPRO-Orange, visualized on the Typhoon 9410 Variable Model Imager with a 488 nm laser and 580 nm filter, and analyzed by densitometry (Image Quant version 5.2). A dimensionless apparent partition coefficient K_x was calculated according to the equation (*33*)

$$K_x = P_b/P_f \times 55.5/0.5[L] \quad (1)$$

where P_b and P_f are the number of moles of bound and free protein, respectively, 0.5[L] is the accessible lipid concentration (outer leaflet only), and the factor 55.5 is the molar concentration of water.

Dynamic Light Scattering (DLS) Measurements. CCT was added from a 5.5 μM stock to a 0.1 mM LUV suspension in buffer A to yield CCT concentrations of 1−300 nM. To check for possible effects on the dispersion state of the samples due to an initial high local concentration of CCT, we reversed the order such that the LUVs were added from a concentrated suspension to a dilute CCT solution. We found that the order of addition had no effect. Light scattering was measured using an ALV DLS/SLS-500 spectrometer/goniometer (ALV-Laser GmbH, Langen, Germany). The sealed sample was placed in a 25 °C toluene bath. The scattered light was detected at a scattering angle of 90° from the transmitted beam; the light source was a 633 nm helium−neon laser.

The quantity measured in DLS is the time autocorrelation function of the scattered intensity $g^{(2)}(\tau)$, where τ is the delay time (*34*). This function can be written in terms of the time autocorrelation function of the scattered field $g^{(1)}(\tau)$

$$g^{(2)}(\tau) = 1 + \beta[g^{(1)}(\tau)]^2 \quad (2)$$

where β is a factor which depends on the experimental geometry.

For monodisperse particles undergoing Brownian motion with a diffusion coefficient D, $g^{(1)}(\tau)$ can be written as $g^{(1)}(\tau) = \exp(-Dq^2\tau)$, where q is the difference between the incident and scattered wave vectors. The diffusion coefficient of the particle is related to its hydrodynamic radius R by the Stokes−Einstein relation

$$D = \frac{K_B T}{6\pi\eta R} \quad (3)$$

where η and T are the viscosity and temperature of the solvent, respectively. The time autocorrelation function hence decays exponentially with a decay rate $\Gamma = Dq^2$.

For polydisperse particles, $g^{(1)}(\tau)$ can be written as

$$g^{(1)}(\tau) = \int_0^\infty G(\Gamma) e^{-\Gamma_\tau} \, d\Gamma \quad (4)$$

where $G(\Gamma)$ describes the distribution of decay rates. Using eqs 2−4, $g^{(2)}(\tau)$ can be written as

$$g^{(2)}(\tau) = 1 + \beta\left[\int_0^\infty G(R) \exp\left(-\frac{K_b T q^2 \tau}{6\pi\eta R}\right) dR\right]^2 \quad (5)$$

The Schulz distribution was used to describe the particle size distribution in this analysis (*35*)

$$G(R) = \frac{R^Z}{Z!}\left(\frac{Z+1}{R_0}\right)^{Z+1} \exp\left[-\frac{R(Z+1)}{R_0}\right] \quad (6)$$

where R_0 is the average radius of the particles and Z is related to the relative standard deviation σ by the relationship $\sigma^2 = 1/(Z+1)$. In this paper, polydispersity is defined as the relative standard deviation, that is, the ratio of the standard deviation to the average radius. The average radius and polydispersity of the particles in the dispersion were determined by fitting eq 5 to the measured intensity−intensity correlation data.

Transmission Electron Microscopy. Negative Staining. CCT−vesicle complexes were prepared by mixing LUVs (1 mM) in 10 mM Tris (pH 7.4), 150 mM NaCl, and 1 mM EDTA with CCT (0.1−1 μM). The samples (8 μL) were pipetted onto copper Formvar coated grids (300 mesh); 1 min was allowed for sample adhesion, and then the excess material was removed by blotting with filter paper. The specimen grid was stained with 8 μL of 2% aqueous uranyl acetate for a few seconds, and the excess stain was removed with filter paper. At least two grids for each sample were examined. All micrographs were digitally recorded in a Hitachi H-760 transmission electron microscope (Hitachi, Tokyo, Japan) operated at 80 kV (University of British Columbia Bioimaging Facility). Pictures were taken at a magnification of 80000×. The diameters of the vesicle aggregates were measured as the largest length of the particle. For large aggregates that significantly deviated from a spherical shape, the diameter determined was the average of the maximal and minimal size. Between 300 and 1300 vesicles for each sample were analyzed. The accuracy of the size determination was ∼10 nm.

Preparation of Gold Particles and Protein−Gold Complexes. Colloidal gold particles with diameters of 7 ± 1 nm (n = 38, SD) were prepared by reduction of tetrachloroauric acid with sodium citrate and tannic acid (*36*). The pH of the gold sol was adjusted to pH ∼7 with K_2CO_3. Gold particles were coated with CCT according to the method of Baschong and Wrigley (*37*) with some modifications. Initially, we used BSA to stabilize the sols; however, the excess of BSA reduced the enzymatic activity of CCT−gold complexes. Therefore, instead of BSA, additional CCT was added to the colloidal gold to an amount that exceeded 5 times the minimal concentration of protein required to stabilize the sol. The protein−gold suspensions were then centrifuged at 32 000 rpm for 60 min, to remove unconjugated CCT, and the pellet containing the CCT−gold complexes was resuspended in 10 mM Tris (pH 7.4), 88 mM NaCl, 1 mM EDTA, and 2 mM DTT. Samples for electron microscopy were prepared following the protocol for negative staining. The lipid:protein ratio in the samples was 1000:1, corresponding to ∼50 CCTs/vesicle.

Reactivity of Gold-Labeled CCT with Antibody against Domain M. Gold-labeled CCT or unlabeled CCT was probed with antibody against residues 256−288 of rat CCTα (anti-domain M) using a dot blot. All steps were carried out at room temperature. One microliter (200−400 ng) of protein sample was spotted onto a strip of hybond ECL nitrocellulose membrane (Amersham Pharmacia Biotech), dried, and

blocked with 0.2% Tween 20 and 6% milk powder in Tris-buffered saline for 1 h. After three washes, the membrane was incubated with a 1:1000 dilution of anti-domain M for 2 h. Subsequently, the membrane blot was washed and incubated overnight with goat anti-rabbit horseradish peroxidase conjugate (1:1000) and detected with enhanced chemiluminescence (Amersham Biosciences). Native CCT was used as a positive control; native and gold-conjugated CCT236 and gold-labeled BSA were used as negative controls.

Vesicle Leakage Assay. LUVs were prepared by extrusion as described above with entrapped self-quenched carboxyfluorescein (80 mM) in 70 mM NaCl, 10 mM Tris (pH 7.4), and 1 mM EDTA. Free CF was removed by chromatography on a Sephadex G 50 column at 4 °C. Vesicles were eluted with 10 mM Tris (pH 7.4), 150 mM NaCl, and 1 mM EDTA, and their integrity was monitored by the stability of CF fluorescence at 520 nm ($\lambda_{ex} = 490$ nm) for 10 min at 20 °C using a PTI Quanta Master Luminescence spectrofluorimeter. Increased fluorescence intensity at 520 nm measured after the addition of CCT or domain M peptide indicated release of vesicle-trapped CF in the bulk solution. To induce complete leakage of CF, vesicles were mixed with Triton X-100 (1%, v/v). The percent of CF leakage was calculated according to the formula (*38*)

$$\% \text{ CF leakage} = [(F - F_0)/(F_T - F_0)] \times 100 \quad (7)$$

where F_0 is the fluorescence before the protein or peptide is added, F is the fluorescence 10 min after the protein or peptide has been added, and F_T is the fluorescence after Triton X-100 has been added.

Fluorescence Resonance Energy Transfer (FRET) Assay for Vesicle Fusion. CCT-induced vesicle lipid mixing was examined using a modification of the method of Struck et al. (*39*). LUVs of PG containing NBD-PE and Rho-PE at 2 mol % each were prepared by extrusion as described above. Labeled vesicles were mixed with a 4-fold molar excess of unlabeled vesicles (total phospholipid concentration of 100 μM), and the NBD-PE fluorescence intensity at 515 nm ($\lambda_{ex} = 460$ nm) was recorded to obtain the baseline (0%) fluorescence. After 5 min, CCT, domain M peptide, or lysozyme was added and the fluorescence intensity was measured for 30 min until a plateau fluorescence value was obtained. Triton X-100 (final concentration of 0.5%) was added to obtain the 100% fluorescence value. Fusion causes a net increase in donor (NBD-PE) and decrease in acceptor (Rho-PE) fluorescence due to dilution of the donor−acceptor pair by nonfluorescent lipids (*39*). All fluorescence measurements were performed at 20 °C in a PTI Quanta Master Luminescence spectrofluorimeter.

RESULTS

CCT Increases the Turbidity of LUVs. In a previous paper, we had noted that CCT promotes an increase in sample turbidity when added to small unilamellar vesicles containing anionic phospholipids (*23*). Figure 2 shows that CCT also increases the turbidity of extruded LUVs composed of the anionic lipid, PG. This is consistent with protein-induced changes in vesicle size due to aggregation, growth, or both. Very low concentrations of CCT corresponding to approximately three CCT monomers per vesicle promoted

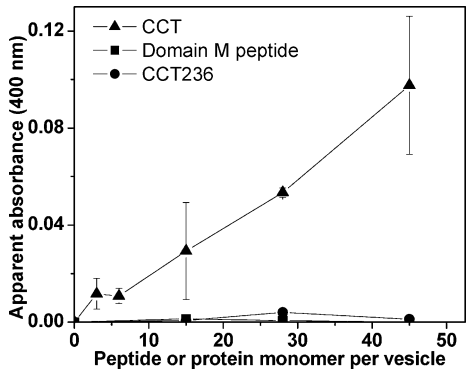

FIGURE 2: Effects of CCT, CCT236, or domain M peptide on vesicle turbidity. The absorbance at 400 nm was monitored. Each point represents a plateau value measured 5 min after addition of the peptide (amino acids 237−293) or purified CCT proteins. The lipid concentration was 100 μM. For the data in this figure and subsequent figures, the ratio of CCT monomer per vesicle was calculated as described in Methods. The data for CCT represent the average of two experiments ± a half-range.

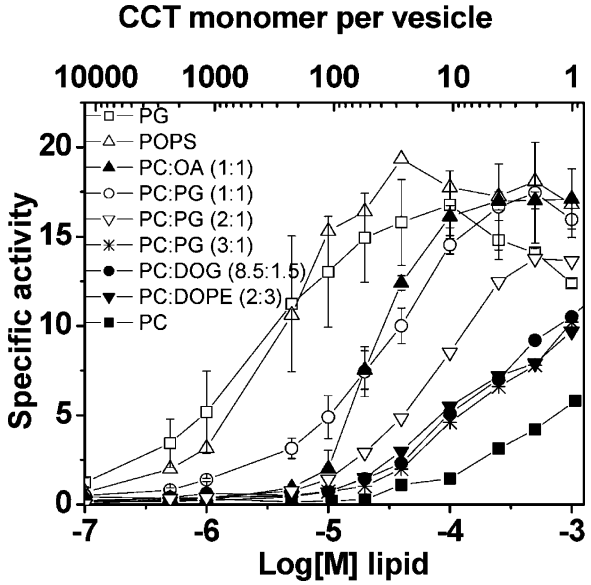

FIGURE 3: Dependence of CCT activity on the lipid concentration of LUVs. The lipid ratios are molar. The concentration of CCT in the assay was 22 nM. In the absence of lipid, the CCT specific activity was 0.24 nmol min^{-1} μg^{-1}. The data are averages ± the error of two or more independent experiments. Specific activity units are nanomoles of CDP-choline formed per minute per microgram of CCT.

turbidity of PG LUVs. Neither the membrane-binding domain M fragment of CCT nor CCT236, the catalytic domain dimer, led to increased turbidity under similar conditions (Figure 2), suggesting that a full-length CCT dimer is required for this effect.

CCT Activation by LUVs. To parallel our investigation of the effects of CCT on the aggregation state of LUVs containing class I and class II lipid activators, we compared the potency of these lipid systems as CCT activators (Figure 3). The LUVs used for both activity measurements and DLS had approximately the same radius (~40 nm). LUVs containing class I lipids (PG and PS) were stronger activators of the enzyme than those containing class II lipids (DOPE and DOG). LUVs of PC were the weakest activators of CCT. The activation curve for PC/OA (1:1) vesicles resembled those of class II lipids at the low concentrations, whereas

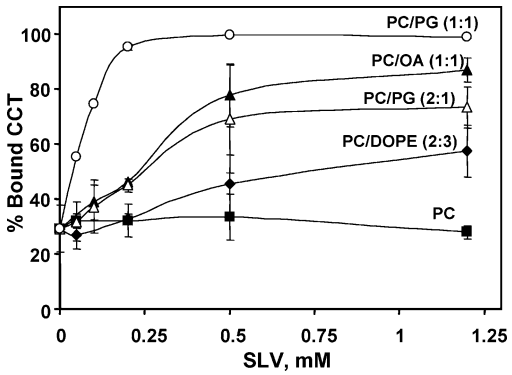

FIGURE 4: Comparison of CCT's binding affinity for SLVs of class I, class II, or PC/OA activators. CCT binding to sucrose-loaded vesicles was assessed as described in Methods. In the absence of lipid, 29 ± 9% of CCT was recovered in the pellet due to sedimentation of CCT or its adhesion to the walls of the tube. The data shown are the average ± the standard deviation from two to four independent measurements.

above 5 μM, it rose steeply and reached half-activation at a vesicle concentration comparable to that for PC/PG (1:1) vesicles. The data also reveal a dependence of CCT activity on the mole percent anionic lipid in the PC/PG mixtures, consistent with previous observations (*2*, *3*).

CCT Has a Lower Affinity for Class II than for Class I Activating Lipids. The potency of a lipid activator isdetermined by the binding strength between CCT and the vesicle containing that activating lipid (*2*−*5*, *11*). Previous direct binding measurements have revealed weaker interactions of domain M peptide to SUVs containing class II compared to class I lipid activators (*4*). Binding of the full CCT enzyme to vesicles containing class I versus class II lipids has not previously been assessed in parallel. Figure 4 compares the affinity of binding of CCT to the class I and class II lipids used in this study. The level of CCT binding to SLVs composed of 100% PC was within the background level in this assay.[2] The apparent partition coefficients, K_x, were calculated from the initial slopes of the binding curves replotted according to eq 1 ($P_b/P_f = K_x \times 0.5[L]/55.5$). K_x values were 1.1, 4.5, 8.3, and 30 $\times$ 10^5 for PC/DOPE (2:3), PC/PG (2:1), PC/OA (1:1), and PC/PG (1:1) vesicles, respectively. The corresponding $\Delta G_{binding}$ values are −6.9, −7.7, −8.0, and −8.8 kcal/mol, respectively. Thus, in agreement with the activity analyses, CCT displayed an ∼30-fold higher affinity for vesicles containing class I lipid activator (PC/PG) than for vesicles containing class II lipid activator (PC/DOPE). The level of binding to PC/OA vesicles was intermediate between those of the two lipid classes.

Dynamic Light Scattering Analysis of Vesicle Size in the Presence of CCT. DLS measurements were performed to quantify CCT-induced changes in vesicle size and polydispersity for LUVs containing class I or II lipid activators. Figure 5 plots the intensity−intensity correlation function of the scattered light (see Methods). The correlation function decays to a baseline with a decay time that depends on the size of the vesicles. The larger the vesicle, the longer the

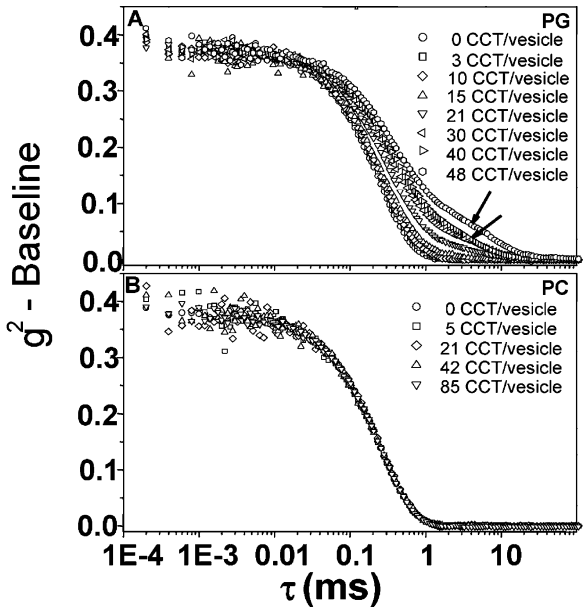

FIGURE 5: Effects of CCT on the light scattering correlation function decay rate for LUVs composed of PG (A) or PC (B). The arrows show the contribution of an extra slow component due to growth of large vesicles that increases with CCT concentration. Data are from one representative set of analyses.

decay time. As few as three CCT monomers per PG vesicle was sufficient to increase the decay time (Figure 5A), whereas even 85 CCT monomers/vesicle did not affect the decay time of PC vesicles (Figure 5B). Figure 5A also shows a contribution to the correlation function of an extra slow component due to growth of large aggregates that increases as the CCT concentration increases (arrows). These results indicate a CCT-induced increase in the size or aggregation state of PG vesicles and no effect of CCT on PC vesicles.

Panels A and C of Figure 6 plot the calculated average radii of the vesicles as a function of CCT concentration determined by fitting eq 5 to the measured intensity−intensity correlation data for all DLS data that did not show an extra slow component in the decay curve. The two classes of lipids exhibited very different responses to CCT. The average particle size measured for vesicles containing the anionic phospholipids PS and PG roughly doubled with 20 CCTs/vesicle compared to zero CCT (Figure 6A). Vesicle polydispersity also increased with an increase in the CCT:vesicle ratio for these systems (Figure 6B), a reflection of the variation in the number of vesicles per aggregate. In contrast, CCT did not cause an increase in the average radii or polydispersity of PC vesicles or of vesicles containing class II activators, DOPE, DOG, and OA (Figure 6A,B). DLS measurements showed that the fragments corresponding to CCT236 and the domain M peptide did not affect the size or the polydispersity of PG LUVs (Figure 6A,B), consistent with their lack of induction of vesicle turbidity (Figure 2). The CCT-induced increase in the extent of vesicle aggregation was dependent on the negative surface charge of the vesicles. The concentration of CCT required to augment vesicle size (Figure 6C) and polydispersity (data not shown) decreased with an increase in mole percent PG in PC/PG LUVs. Aggregation was detected only with PC/PG LUVs containing ≥33 mol % anionic lipid. Previous studies have shown a similar threshold concentration for PG promoting

[2] The apparent discrepancies between the lipid potency reflected in the binding measurements (Figure 4) versus the activity measurements (Figure 3) are due to differing vesicle diameters of the SLVs used for binding (∼200 nm diameter) versus the LUVs used for activity (80 nm diameter). When binding and activity are assessed using the same lipid vesicle system, there is close agreement in lipid potency (*3*).

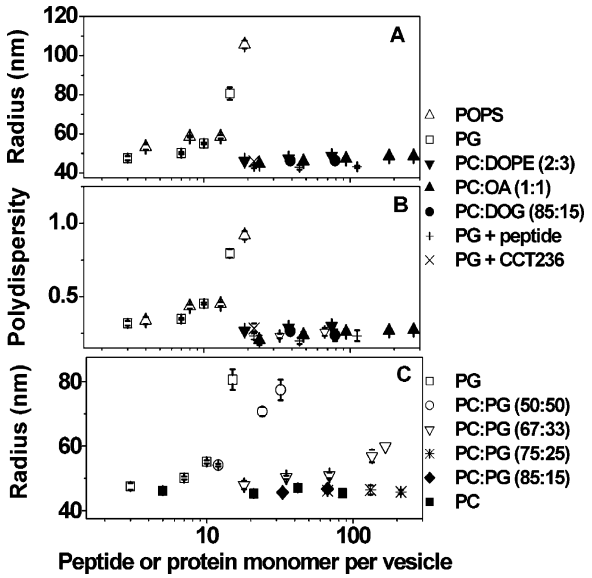

FIGURE 6: Effects of CCT, CCT236, or domain M peptide (peptide) on the average radius (A and C) and polydispersity (B) of LUVs. The average radius was derived from the DLS data in Figure 5, for correlation function decay curves that did not exhibit the extra slow component. The polydispersity (B) is the standard deviation of the radius divided by the average radius, as described in Methods. (C) Dependence of vesicle radius on the mole percent anionic phospholipid. CCT was used in the experiments shown in this panel. Data in panels A−C are averages of five measurements taken for each sample. In most cases, the standard deviation bars are within the size of the symbols.

binding of CCT to SLVs at pH 7.4 and similar ionic strength (*3*).

Changes in the Aggregation State of CCT−LUV Complexes As Revealed by TEM. TEM was used to confirm the DLS data suggesting an effect of CCT on PG vesicle size. Moreover, TEM would allow direct visualization of the effects of CCT on the size and potentially the morphology of the vesicles containing class I or class II lipid or OA. Panels A and D of Figure 7 show representative micrographs of PG and PC/OA LUVs in the absence of protein. Before addition of CCT, the vesicles appeared to be dispersed well and relatively nonaggregated. There were some clusters within which the individual vesicles could be discerned.

The addition of CCT, corresponding to 6−10 monomers per PG vesicle (Figure 7B), induced vesicle clustering and the formation of aggregates with flattened contact areas. In some of these aggregates, individual vesicles appeared to be merged (Figure 7B, arrows). In addition, we observed a small population of very large (micrometer) aggregates that most likely resulted from vesicles that had fused (Figure 7C). In contrast, addition of up to 29 CCTs per vesicle did not affect the aggregation state or size of PC/OA vesicles (Figure 7E,F). We did not observe large (micrometer) aggregates in any of the CCT−PC/OA samples examined under the microscope.

The size distributions of PG and PC/OA vesicles before and after the addition of CCT were derived from the micrographs of stained vesicle preparations (Figure 8). PG and PC/OA vesicles in the absence of CCT were fairly uniform in size with mean radii ± the standard deviation of 47 ± 24 (N = 607) and 62 ± 25 nm (N = 300), similar to the medians, 45 and 60 nm, respectively (Figure 8A,B, white bars). CCT shifted the size distribution of PG vesicles toward

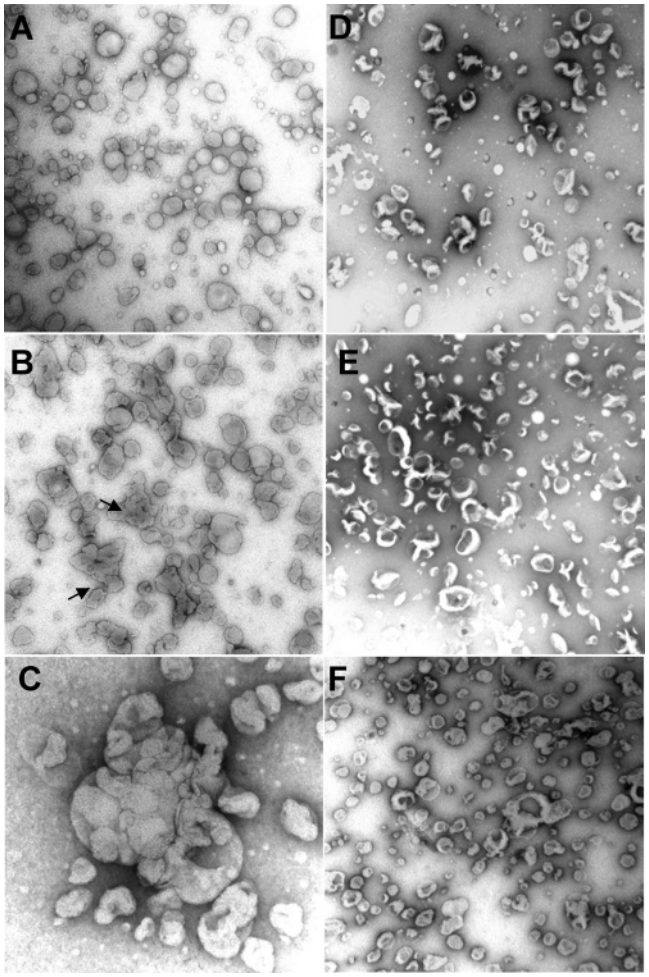

FIGURE 7: Effect of CCT on the dispersion state of LUVs, monitored by TEM. Transmission electron micrographs of negatively stained LUVs were prepared as described in Methods: (A) PG LUVs, (B) PG LUVs with 10 CCTs/vesicle, (C) PG LUVs with 29 CCTs/vesicle, (D) PC/OA (1:1) LUVs, (E) PC/OA (1:1) LUVs with 6 CCTs/vesicle, and (F) PC/OA (1:1) LUVs with 29 CCTs/vesicle. Arrows in panel B indicate small aggregates, and panel C shows a large (micrometer) aggregate of PG vesicles. The scale bar equals 300 nm for panels A, B, and D−F and 100 nm for panel C.

larger particles at all concentrations that were studied. With six CCT monomers per vesicle, the mean particle radius was 79 ± 86 nm, and ~13% of all vesicles had radii greater than the largest radius observed in the pure PG vesicle population (Figure 8A, black bars). Similar size distributions and increases were seen with 10 and 29 CCT monomers/vesicle (data not shown). CCT did not cause significant changes in the size distribution of PC/OA vesicles: in the presence of a 10-fold higher concentration of CCT (75 CCTs/vesicle), only ~1.5% of the total vesicles had radii larger than the biggest particles seen in PC/OA samples without CCT (Figure 8B).

The mean radii obtained from the histograms were compared with those determined by DLS. Quantitative agreement exists between EM and DLS on the size of PG vesicles without CCT. Both techniques showed a CCT-dependent increase in the size and polydispersity of PG vesicles, but no effect of CCT on PC/OA vesicles (Figures 6 and 8). The size of PC/OA vesicles determined from EM, 62 ± 25 nm, was slightly larger than the value (45.9 ± 8.2 nm) measured by DLS. In the EM images used for the

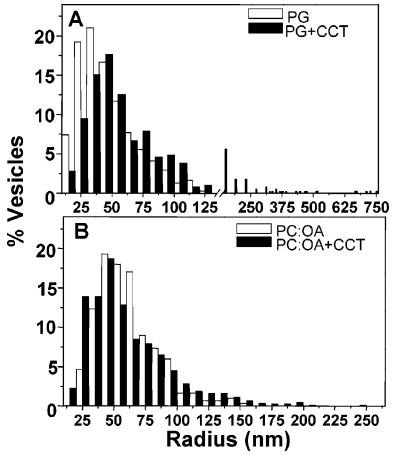

FIGURE 8: Effect of CCT on the size distribution of vesicles measured from electron micrographs of negatively stained samples. Histograms were prepared by manual measurement of 300−1300 vesicles for each condition: (A) PG LUVs without (white bars) and with 6 CCTs/vesicle (black bars). (B) PC/OA LUVs without (white bars) and with 75 CCTs/vesicle (black bars).

calculations, the PC/OA vesicles were slightly elongated and invaginated (Figure 7D), and since we measured the largest length of the particles, an overestimation of the radii of the vesicles is probable. The extrusion process itself may generate nonspherical LUVs (*40*), and the EM preparation deforms them, thus thwarting an assessment of morphology differences between the two lipid classes.

Direct Visualization of Gold-Labeled CCT Bound to Vesicle Aggregates. To directly visualize the association of CCT with vesicle surfaces, and to probe whether CCT accumulates at points of vesicle contact, we prepared CCT conjugated to 7 nm colloidal gold. Stable CCT−gold sols were formed as judged by TEM observations that showed the absence of aggregates (Figure 9C). The size of a CCT dimer, which can be approximated on the basis of determined structures of a homologous glycerophosphate cytidylyltransferase (*20*) and domain M (*22*), is on the same order of magnitude as the 7 nm gold particles. Thus, only one or two CCT molecules can bind to each gold particle. Moreover,

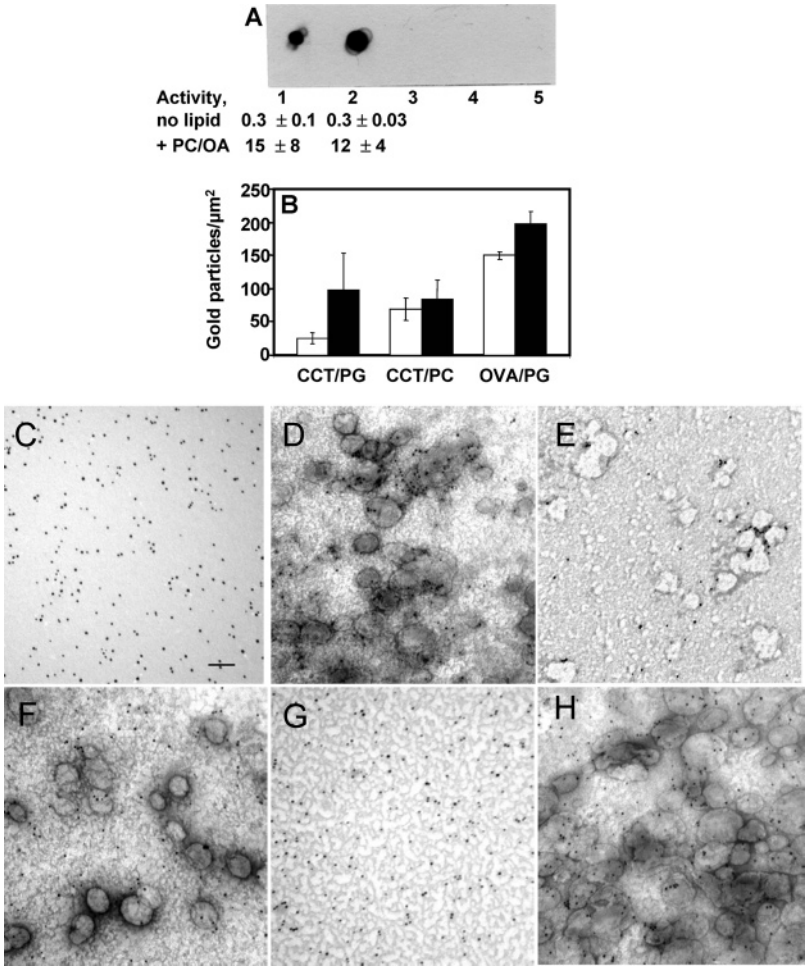

FIGURE 9: (A) Gold conjugation does not render the domain M inaccessible. Proteins were immobilized onto hybond ECL nitrocellulose membrane, and their reaction with the anti-domain M antibody was tested: lane 1, native CCT (250 ng); lane 2, gold-labeled CCT (400 ng); lane 3, native CCT236 (200 ng); lane 4, gold-labeled CCT236; and lane 5, gold-labeled BSA. Samples 3−5 are negative controls showing that the anti-M reactivity is specific for domain M, and is not a reaction with nonepitopic domains on CCT or with the gold particle. The activity (nanomoles of CDP-choline per minute per microgram) of native and gold-conjugated CCT was measured with or without 100 μM PC/OA SUVs. (B) Density of gold-labeled CCT and ovalbumin (OVA) in PG and PC LUVs. The means ± the standard deviation of the distributions of gold particles densities are plotted for 20 (CCT/PG), 14 (CCT/PC), and 4 (OVA/PG) micrographs. The *t*-test values are 5.55 ($p = 0.001$), 1.72 ($p = 0.1$), and 4.65 ($p = 0.01$) for the three systems, respectively. The total number of gold particles counted for each system was 2132 (CCT/PG), 2138 (CCT/PC), and 1660 (OVA/PG). White bars and black bars represent densities for vesicle-free and vesicle-covered areas in the micrographs, respectively. (C−H) Transmission electron micrographs show accumulation of gold-conjugated CCT on aggregated PG vesicles: gold-conjugated CCT in the absence of vesicles (C) and in the presence of PG (D and E; the two images are from separate LUV and CCT−gold preparations) or PC (F) LUVs. Panels G and H show gold-conjugated ovalbumin in the absence and presence of PG LUVs, respectively. The scale bar is 100 nm.

most of the gold particles labeled with CCT were monodisperse (Figure 9C), indicating that only one particle binds to each CCT molecule.

The process of conjugation did not affect the ability of CCT to bind to antibody directed against domain M (Figure 9A). In addition, gold conjugation did not block the ability of PC/OA vesicles to stimulate CCT activity (Figure 9A). Thus, domain M remains accessible in the CCT−gold complex. Negative staining of PG and PC vesicles incubated with the CCT−gold complex (∼50 CCT monomers/vesicle) revealed gold particles associated with vesicles and in the background (Figure 9D−F). We did not wash the grids after deposition of the vesicle/CCT−gold mixture because washing released most of the material (including the LUVs) from the grid. Despite this, the CCT−gold complex was not evenly distributed on the micrographs, but was preferentially associated with PG vesicles. To quantify the amount of vesicle labeling, images for each sample were selected randomly, individual CCT−gold particles were counted, and their density in vesicle-free and vesicle-covered areas of the micrographs was determined (Figure 9B). There was an ∼4-fold increase in the density of CCT−gold complexes associated with PG LUVs, compared to an only ∼1.2-fold enrichment of CCT−gold complexes bound to PC LUVs. To address potential nonspecific adherence of the gold particles to the vesicle surface, we initially attempted to visualize gold-labeled CCT236, missing domains M and P. However, despite numerous attempts using different conditions, we were unable to prepare stable conjugates of the CCT236−gold complex. Ovalbumin−gold conjugates (Figure 9G) were readily prepared and were used as a control protein in experiments with PG LUVs (Figure 9H). The ratio of gold density in vesicle-covered to vesicle-free areas was 1.3, similar to the value for CCT−gold/PC LUVs (Figure 9B). Therefore, we conclude that there was a significant enrichment of CCT−gold complexes associated with PG, but not PC, vesicles, consistent with the activity and binding data of Figures 3 and 4 and published data (*2*−*5*, *21*, *23*).

Most notably, the images revealed an accumulation of CCT−gold particles on aggregated PG vesicles. Within these aggregates, CCT−gold particles were generally distributed both on the peripheral vesicle surfaces and in sites of close membrane apposition (Figure 9D). In some images, there was a clear accumulation of gold particles at contact sites between vesicles of the aggregate, supporting a cross-bridging mechanism for the interaction of CCT with PG vesicles (Figure 9E). This accumulation between two vesicles was not noted in samples containing PC LUVs.

CCT Induces Membrane Destabilization of Anionic LUVs. DLS and TEM analyses showed a clear difference in the aggregation potential of class I and class II lipid vesicles. To further characterize these differences, we investigated the CCT-induced perturbation of bilayer stability using two methods. First, we tested the leakage of vesicle-entrapped carboxyfluorescein (CF) upon addition of CCT to class I and class II lipid vesicles. Binding of CCT to vesicles containing class I lipids (PG and PC/PG) strongly destabilized the bilayer as shown by the release and dequenching of CF (Figure 10A). At ∼20 CCT monomers per PG vesicle, the fluorescence was near maximal (∼70%). The membrane-destabilizing potential of CCT was dependent on the percent of anionic phospholipids. On the other hand, CCT had little

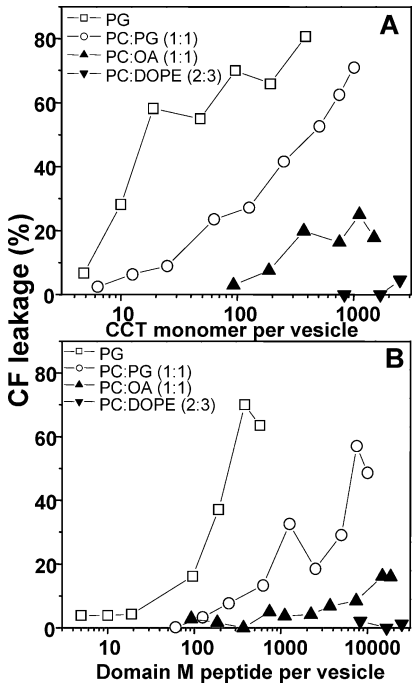

FIGURE 10: CCT and domain M peptide differentially destabilize bilayers. Effects of CCT (A) and domain M peptide (B) on vesicle content leakage were monitored by the increase in the fluorescence of vesicle-entrapped CF. Lipid ratios are molar. The concentration of lipid was 20 μM. CF fluorescence was measured 10 min after addition of the protein or peptide when plateau values were reached.

effect on CF release from vesicles containing class II lipids (PC/DOPE). The perturbing effect of CCT on PC/OA vesicles was intermediate. Thus, CCT interaction with the two classes of lipid vesicles has a very different impact on bilayer integrity, which is likely related to the different CCT−lipid binding affinities (Figure 4).

We also examined whether the domain M peptide can induce CF leakage. Figure 10B shows that while it was effective at releasing CF, roughly 10 times more peptide per vesicle was required to reach maximal fluorescence compared to full-length CCT. This suggests that the bilayer perturbing properties of domain M in the intact CCT differ from those of the fragment. The partition coefficients for a domain M-based peptide binding to PC/OA (1:1) and PC/PG (1:1) SUVs (*4*) are similar to those determined for binding of full-length CCT to SLVs of the same compositions (Figure 4). Therefore, the observed differences may not reflect different membrane binding affinities of CCT and domain M peptide. Rather, the dimeric structure of CCT may contribute to the enhanced bilayer perturbation. Although the full-length CCT enzyme was a much more potent bilayer destabilizer than the domain M peptide, the rank order of responsiveness between the lipid classes was similar. Class I lipids were the most sensitive; class II lipids (DOPE) were insensitive, and PC/OA vesicles exhibited intermediate sensitivity. This supports the concept that the lipid affinity of domain M governs the interaction of CCT with activating lipids (*4*, *23*).

Second, we examined the effect of CCT and domain M peptide on intervesicular lipid mixing of PG LUVs using a FRET assay. CCT did not induce significant lipid mixing in the range of concentrations used in the vesicle aggregation and contents leakage experiments (1−100 monomers/vesicle): there was an only ∼1−3% increase in the

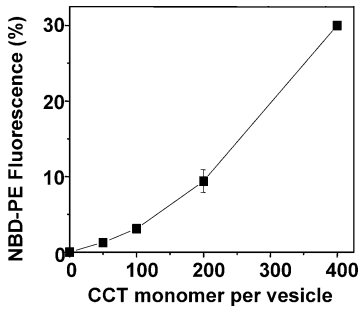

FIGURE 11: CCT-induced lipid mixing of PG LUVs monitored by FRET. The increase in the fluorescence intensity of NBD-PE (donor) at 515 nm was measured for 30 min after the addition of CCT. The fluorescence intensity is normalized to the fluorescence associated with 100% mixing upon solubilization with Triton X-100. The vesicle concentration was 100 μM. Data are averages of two experiments. The error range falls within the size of the symbol for some points.

fluorescence of NBD-PE (Figure 11). The fusogenic protein, lysozyme (*38*), also exhibited an only 1−2% increase in the NBD-PE fluorescence at these same low protein:lipid ratios (data not shown). At higher concentrations of 200−400 CCTs/vesicle, we measured 10−30% fluorescence increases (Figure 11). At these concentrations, corresponding to protein:lipid molar ratios of 0.004−0.008, the lipid mixing activity of CCT was comparable to that reported for fusogenic peptides, such as the HIV GP41 C-terminal fusion peptide (*41*), and the transmembrane segments of the SNARES, synaptobrevin II, and syntaxin 1A (*42*). Thus, the pronounced induction of aggregation and leakiness of anionic vesicles observed at low CCT:vesicle ratios was not associated with significant membrane fusion; however, CCT has lipid mixing activity at protein:lipid ratios comparable to those of other fusogenic peptides and proteins. Domain M peptide did not have fusogenic activity at up to 2000 peptides/vesicle (data not shown), in keeping with its inability to induce aggregation, a necessary step for fusion.

DISCUSSION

CCT Mediates Cross Bridging of Vesicles Containing Anionic Phospholipids. In this study, we used three complementary methods to assess the CCT-induced aggregation of LUVs: vesicle apparent absorbance, dynamic light scattering, and TEM. All three approaches were consistent in showing that only one to three CCT dimers per vesicle ($\sim 10^4$ lipid:CCT molar ratio) suffice to induce aggregation of LUVs composed of anionic phospholipids, but not LUVs composed of PC and OA or class II lipids.

Some proteins, for example, annexin IV (*43*), myelin proteolipid (*44*), and cytochrome *c* (*45*), induce vesicle aggregation by coating the vesicle surface, which leads to protein oligomerization (*43*, *44*) and/or vesicle charge neutralization (*45*). However, the low CCT:vesicle ratio required to induce aggregation and the inability of the membrane binding domain on its own to induce aggregation clearly indicate that this mechanism does not apply to CCT-induced aggregation. The requirement for the N-terminal dimerization domain plus domain M argues in favor of a cross-bridging mechanism for aggregation, in which the M domains of each subunit are positioned on opposite sides of the CCT dimerization domains (Figure 1B). The use of CCT−gold complexes directly showed preferential association of CCT with vesicle membranes and accumulation of CCT over aggregated PG vesicles. In some images, we observed accumulation of CCT−gold particles at membrane−membrane contacts (Figure 9E), thus supporting CCT-induced cross bridging of vesicles. Our data also suggest that vesicle aggregation is not merely a consequence of bilayer packing perturbation. The domain M peptide did not induce vesicle aggregation when added to PG LUVs at a concentration as high as 4000 peptides/vesicle, whereas bilayer packing disruption occurred with as little as 100 peptides/vesicle (Figure 10B).

That CCT can cross-bridge vesicles composed of class I lipids suggests a model for CCT domain organization in which the two M domains can position themselves on opposite poles of the catalytic dimer as depicted in Figure 1B. However, our data do not exclude single-bilayer engagement of both M domains as depicted in Figure 1A. If the linker between the catalytic domain and domain M is flexible, as indicated in Figure 1, both the cross-bridging mode (Figure 1B) and the single-bilayer binding mode (Figure 1A) should be possible. Restriction of the translational freedom of the two bridged vesicles would dictate that only a strong interaction between the enzyme and membrane would allow the cross-bridging mode.

The CCT Dimer Does Not Cross-Bridge Vesicles Containing Class II Lipids. CCT did not promote aggregation of LUVs containing the class II lipids, DOG or DOPE, even at CCT:vesicle ratios as high as 80 (Figure 6). The most likely explanation for the different response of class I versus class II lipids is the weaker energetics of binding of CCT to these lipid vesicles. The apparent partition coefficients calculated from the binding isotherms (Figure 4) indicate ~30-fold higher affinity of CCT for PC/PG vesicles than for PC/DOPE vesicles. This is consistent with an electrostatic contribution of 2 kcal/mol calculated for the binding of a domain M peptide to PC/PG (1:1) versus PC vesicles (*4*), but a curvature elastic stress contribution of only 0.4 kcal/mol, based on comparison of CCT activation by DOPC/DOPE (1:1) versus DOPC vesicles (*10*). CF leakage experiments also indicated weaker interactions of CCT and domain M peptide with PC/DOPE LUVs than with PC/PG LUVs (Figure 10A,B). Weak association of CCT via domain M with membranes containing class II lipids may result in short-lived complexes that dissociate faster than the time scale of cross bridging and aggregation. The stronger binding of CCT to anionic vesicles may enable the coupling of longer-lived interactions to aggregation. Such an explanation is in accord with comparisons of the relative kinetics of binding (fast) versus aggregation (slow) of myelin basic protein (*46*) and mitochondrial creatine kinase octamer (*47*). A CCT:vesicle ratio of 80 only marginally increased the radius of vesicles containing 50% OA or 33% PG (10 or 15% increase, respectively). The partition coefficient of CCT for binding to either of these vesicles was in the range of $5-8 \times 10^5$, corresponding to a $\Delta G_{binding}$ of −7.7 to −8 kcal/mol. Thus, the binding strength must exceed 8 kcal/mol for generation of stable vesicle aggregates tethered by CCT. For vesicle interactions weaker than this, CCT could engage membranes as depicted in Figure 1A. Alternatively, the CCT domain organization depicted in Figure 1B may dominate, leading to only one domain M of the CCT dimer engaged with a bilayer.

The Cross-Bridging Vesicle Interaction Is Not Required for CCT Activation. CCT is clearly activated by OA and by class II lipids, although they are less potent than class I lipids (Figure 3; *2*, *3*, *11*). The data in Figure 3 clearly show that the enzyme can be fully activated when engaging PC/OA (1:1) vesicles in a non-cross-bridging mode. The steep activation curve by OA-containing vesicles (Figure 3) may result from the synergistic combination of its weak negative charge in bilayers (*48*) and its negative curvature strain effects (*49*, *50*). Synergism between these two features has been observed in activation and binding analyses with vesicles containing low levels of anionic lipids and diacylglycerol (*2*). The question of the consequences of engagement of one versus two M domains on CCT activity remains, irrespective of whether the binding arrangement is cross-bridging. Is engagement of one domain M sufficient for full activation, half, or none? The answer might be approached by analysis of CCT heterodimers containing only one functional domain M.

Biological Implications: The Potential Participation of CCT in Cellular Events that Involve Membrane Apposition. The potential participation of CCT in cellular events that involve membrane apposition was examined. The property of CCT to mediate membrane apposition is a new aspect of the interactions of CCT with lipid bilayers that has not been addressed previously. The work we present here raises many questions. The most intriguing is whether the ability of CCT to promote cross bridging of lipid membranes containing anionic lipids has bearing on the in vivo functions of the enzyme. A minimum of ~30 mol % anionic phospholipid was required to observe aggregation in vitro (Figure 6). ER and nuclear membranes where CCT is engaged contain 20−30 mol % anionic lipid (*17*, *18*). This establishes the potential for CCT to cross-bridge cell membranes which occur in close apposition, possibly promoting that apposition in combination with a second tethering protein. Low-affinity monomer−monomer protein interactions can suffice to bring apposed membranes together in vivo. Overexpressed green fluorescent protein, which undergoes head-to-tail dimerization, when fused to the transmembrane domains of ER resident proteins can induce cross bridging of ER membranes and the formation of stacked membrane structures in cells (*51*). CCT's dimer interaction is by contrast very strong, requiring complete protein denaturation for dissociation to monomers (S. Taneva, unpublished results).

There are numerous examples of proteins that function in cells to tether membranes that also aggregate phospholipid vesicles in vitro. The acrosomal sperm protein, bindin, is involved in adhesion and fusion of sperm−egg plasma membranes during fertilization (*52*, *53*). Annexin II (*54*) is implicated in docking and fusion of lamellar bodies to the plasma membrane during exocytosis of lamellar bodies from alveolar epithelial type II cells (*55*). Myelin basic protein anchors the cytoplasmic face of two apposed bilayers of the myelin sheath (*56*, *57*). Surfactant protein A participates in membrane tethering of multilamellar aggregates of lung surfactant (*58*, *59*). SNARES also induce vesicle aggregation in vitro (*60*).

CCT's function in the regulation of PC synthesis does not immediately offer an explanation for a role as a membrane tether. However, the idea of communication between PC synthesis and vesicular transport has emerged from many studies in diverse systems (*61*−*63*). CCT null mutations bypass the requirement for Sec14p in yeast (*64*) or Nir2 in mammalian cells (*65*), essential proteins for secretion from the Golgi (*64*, *65*), suggesting an inhibitory role of CCT in vesicular traffic (*61*). Nir2 can form a complex with a SNARE-like protein, VAP-B, to promote expansion of ER, and this complex has been proposed to tether the apposed membranes of the stacked ER (*66*). A more direct connection to tethering is the observation of an interaction of CCT in vitro with p115 (*67*), a vesicle-tethering golgin associated with COPI and COPII vesicles in ER ↔ Golgi traffic (*68*). Conceivably, CCT's vesicle tethering property might facilitate its interaction with p115 and/or Nir2.

ACKNOWLEDGMENT

We thank G. Martens, D. Horne, and Dr. E. Humphrey, University of British Columbia Bioimaging Facility, for their valuable advice and suggestions with the TEM and gold labeling, as well as provision of some materials for the gold labeling. We thank Dr. Joanne Johnson for preparing the purified CCT.

REFERENCES

1. Cornell, R. B., and Northwood, I. C. (2000) Regulation of CTP: phosphocholine cytidylyltransferase by amphitropism and relocalization, *Trends Biochem. Sci. 25*, 441−447.
2. Arnold, R. S., and Cornell, R. B. (1996) Lipid regulation of CTP: phosphocholine cytidylyltransferase: Electrostatic, hydrophobic, and synergistic interactions of anionic phospholipids and diacylglycerol, *Biochemistry 35*, 9917−9924.
3. Arnold, R. S., De Paoli-Roach, A., and Cornell, R. B. (1997) Binding of CTP:phosphocholine cytidylyltransferase to lipid vesicles: Diacylglycerol and enzyme dephosphorylation increase the affinity for negatively charged membranes, *Biochemistry 36*, 6149−6156.
4. Johnson, J. E., Rao, N. M., Hui, S.-W., and Cornell, R. B. (1998) Conformation and lipid binding properties of four peptides derived from the membrane-binding domain of CTP:phosphocholine cytidylyltransferase, *Biochemistry 37*, 9509−9519.
5. Johnson, J. E., Xie, M., Sing, L. M., Edge, R., and Cornell, R. B. (2003) Both acidic and basic amino acids in an amphitropic enzyme, CTP:phosphocholine cytidylyltransferase, dictate its selectivity for anionic membranes, *J. Biol. Chem. 278*, 514−522.
6. Cornell, R. B., and Vance, D. E. (1987) Translocation of CTP: phosphocholine cytidylyltransferase from cytosol to membranes in HeLa cells: Stimulation by fatty acid, fatty alcohol, mono- and diacylglycerol, *Biochim. Biophys. Acta 919*, 26−36.
7. Wang, Y., MacDonald, J. I. S., and Kent, C. (1993) Regulation of CTP:phosphocholine cytidylyltransferase in HeLa cells. Effect of oleate on phosphorylation and intracellular localization, *J. Biol. Chem. 268*, 5512−5518.
8. Jamil, H., Hatch, G., and Vance, D. E. (1993) Evidence that binding of CTP:phosphocholine cytidylyltransferase to membranes in rat hepatocytes is modulated by the ratio of bilayer- to non-bilayer-forming lipids, *Biochem. J. 291*, 419−427.
9. Utal, A., Jamil, H., and Vance, D. E. (1991) Diacylglycerol signals the translocation of CTP:choline-phosphate cytidylyltransferase in HeLa cells treated with 12-O-tetradecanoylphorbol-13-acetate, *J. Biol. Chem. 266*, 24084−24091.
10. Attard, G. S., Templer, R. H., Smith, W. S., Hunt, A. N., and Jackowski, S. (2000) Modulation of CTP:phosphocholine cytidylyltransferase by membrane curvature elastic stress, *Proc. Natl. Acad. Sci. U.S.A. 97*, 9032−9036.
11. Davies, S. M. A., Epand, R. M., Kraayenhof, R., and Cornell, R. B. (2001) Regulation of CTP:phosphocholine cytidylyltransferase activity by the physical properties of lipid membranes: An important role for stored curvature strain energy, *Biochemistry 40*, 10522−10531.
12. Watkins, J. D., and Kent, C. (1992) Immunolocalization of membrane-associated CTP:phosphocholine cytidylyltransferase in phosphatidylcholine-deficient Chinese hamster ovary cells, *J. Biol. Chem. 267*, 5686−5692.

13. Lagace, T. A., Story, M. K., and Ridgeway, N. D. (2000) Regulation of phosphatidylcholine metabolism in Chinese hamster ovary cells by the sterol regulatory element-binding protein (SREBP)/SREBP cleavage-activating protein pathway, *J. Biol. Chem. 275*, 14367−14374.
14. Lagace, T. A., and Ridgway, N. D. (2005) The rate-limiting enzyme in phosphatidylcholine synthesis regulates proliferation of the nucleoplasmic reticulum, *Mol. Biol. Cell 16*, 1120−1130.
15. Northwood, I. C., Tong, A. H., Crawford, B., Drobnies, A. E., and Cornell, R. B. (1999) Shuttling of CTP:phosphocholine cytidylyltransferase between the nucleus and endoplasmic reticulum accompanies the wave of phosphatidylcholine synthesis during the G_0 to G_1 transition, *J. Biol. Chem. 274*, 26240−26248.
16. Lykidis, A., Baburina, I., and Jackowski, S. (1999) Distribution of CTP:phosphocholine cytidylyltransferase (CCT) isoforms. Identification of a new CCTβ splice variant, *J. Biol. Chem. 274*, 26992−70001.
17. D'Antuono, C., del Carmen Fernández-Tomé, M., Sterin-Speziale, N., and Bernik, D. L. (2000) Lipid−protein interactions in rat renal subcellular membranes: A biophysical and biochemical study, *Arch. Biochem. Biophys. 382*, 39−47.
18. Neitcheva, T., and Peeva, D. (1995) Phospholipid composition, phospholipase A2 and sphingomyelinase activities in rat liver nuclear membrane and matrix, *Int. J. Biochem. Cell Biol. 27*, 995−1001.
19. Cornell, R. B. (1989) Chemical cross-linking reveals a dimeric structure for CTP:phosphocholine cytidylyltransferase, *J. Biol. Chem. 264*, 9077−9081.
20. Weber, C. H., Park, Y. S., Sanker, S., Kent, K., and Ludwig, M. (1999) A prototypical cytidylyltransferase: CTP:glycerol-3-phosphate cytidylyltransferase from *Bacillus subtilis*, *Structure 7*, 1113−1124.
21. Xie, M., Smith, J. L., Ding, Z., Zhang, D., and Cornell, R. B. (2004) Membrane binding modulates the quaternary structure of CTP:phosphocholine cytidylyltransferase, *J. Biol. Chem. 279*, 28817−28825.
22. Dunne, J. S., Cornell, R. B., Johnson, J. E., Glover, N. R., and Tracey, A. S. (1996) Structure of the membrane binding domain of CTP:phosphocholine cytidylyltransferase, *Biochemistry 35*, 11975−11984.
23. Taneva, S., Johnson, J. E., and Cornell, R. B. (2003) Lipid-induced conformational switch in the membrane binding domain of CTP: phosphocholine cytidylyltransferase: A circular dichroism study, *Biochemistry 42*, 11768−11776.
24. MacDonald, J. I., and Kent, C. (1994) Identification of phosphorylation sites in rat liver CTP:phosphocholine cytidylyltransferase, *J. Biol. Chem. 269*, 10529−10537.
25. Wang, Y., and Kent, C. (1995) Effects of altered phosphorylation sites on the properties of CTP:phosphocholine cytidylyltransferase, *J. Biol. Chem. 270*, 17843−17849.
26. Yang, W., and Jackowski, S. (1995) Lipid activation of CTP: phosphocholine cytidylyltransferase is regulated by the phosphorylated carboxyl-terminal domain, *J. Biol. Chem. 270*, 16503−16506.
27. Wang, Y., and Kent, C. (1995) Identification of an inhibitory domain of CTP:phosphocholine cytidylyltransferase, *J. Biol. Chem. 270*, 18948−18952.
28. Friesen, J. A., Campbell, H. A., and Kent, C. (1999) Enzymatic and cellular characterization of a catalytic fragment of CTP: phosphocholine cytidylyltransferase α, *J. Biol. Chem. 274*, 13384−13389.
29. Bartlett, G. R. (1959) Phosphorus assay in column chromatography, *J. Biol. Chem. 234*, 466−468.
30. Houslay, M. D., and Stanley, K. K. (1982) *Dynamics of biological membranes: Influence of synthesis, structure and function*, Willey, New York.
31. Evans, R. W., Williams, M. A., and Tinoco, J. (1987) Surface areas of 1-palmitoyl phosphatidylcholines and their interactions with cholesterol, *Biochem. J. 245*, 455−462.
32. Ha, T. H., Kim, D. K., Choi, M.-U., and Kim, K. (2000) Influence of poly(ethylenimine) on the monolayer of oleic acid at the air/water Interface, *J. Colloid Interface Sci. 226*, 98−104.
33. Tamm, L. K. (1994) Physical Studies of Peptide-Bilayer Interactions, in *Membrane Protein Structure* (White, S. H., Ed.) pp 283−313, Oxford University Press, New York.
34. Berne, B. J., and Pecora, R. (1990) *Dynamic Light Scattering*, Robert E. Krieger Publishing Co.: Melbourne, Florida.
35. Hallet, F. R., Nickel, B., Samuels, C., and Krygsman, P. H. (1991) Determination of vesicle size distribution by freeze fracture electron microscopy, *J. Electron Microsc. Tech. 17*, 459−466.
36. Slot, J. W., and Geuze, H. J. (1985) A new method of preparing gold probes for multiple-labeling cytochemistry, *Eur. J. Cell Biol. 38*, 87−93.
37. Baschong, W., and Wrigley, N. G. (1990) Small colloidal gold conjugated to Fab fragments or to immunoglobulin G as high-resolution labels for electron microscopy: A technical overview, *J. Electron Microsc. Tech. 14*, 313−323.
38. De Arcuri, B. F., Vechetti, G. F., Chehin, R. N., Goni, F. M., and Morero, R. D. (1999) Protein-induced fusion of phospholipid vesicles of heterogeneous sizes, *Biochem. Biophys. Res. Commun. 262*, 586−590.
39. Struck, D. K., Hoekstra, D., and Pagano, R. E. (1981) Use of resonance energy transfer to monitor membrane fusion, *Biochemistry 20*, 4093−4099.
40. Mui, B. L.-S., Cullis, P. R., Evans, E. A., and Madden, T. D. (1993) Osmotic properties of large unilamellar vesicles prepared by extrusion, *Biophys. J. 64*, 443−453.
41. Suarez, T., Gallaher, W. R., Agirre, A., and Goni, F. M. (2000) The pre-transmembrane region of the human immunodeficiency virus type-1 glycoprotein: A novel fusogenic sequence, *J. Virol. 74*, 8038−8047.
42. Langosch, D., Crane, J. M., Brosig, B., Hellwig, A., Tamm, L. K., and Reed, J. (2001) Peptide mimics of SNARE transmembrane segments drive membrane fusion depending on their conformational plasticity, *J. Mol. Biol. 311*, 709−721.
43. Kaetzel, M. A., Mo, Y. D., Mealy, T. R., Campos, B., Bergsma-Schutter, W., Brisson, A., Dedman, J. R., and Seaton, B. A. (2001) Phosphorylation mutants elucidate the mechanism of annexin IV-mediated membrane aggregation, *Biochemistry 40*, 4192−4199.
44. Bizzozero, O. A., and Howard, T. A. (2002) Myelin proteolipid protein-induced aggregation of lipid vesicles: Efficacy of the various molecular species, *Neurochem. Res. 27*, 1269−1277.
45. Bernad, S., Oellerich, S., Soulimane, T., Noinville, S., Baron, M.-H., Paternostre, M., and Lecomte, S. (2004) Interaction of horse heart and thermus thermophilus type cytochromes with phospholipid vesicles and hydrophobic surfaces, *Biophys. J. 86*, 3863−3872.
46. Ter Beest, M. B. A., and Hoekstra, D. (1993) Interaction of myelin basic protein with artificial membranes. Parameters governing binding, aggregation and dissociation, *Eur. J. Biochem. 211*, 689−696.
47. Stachowiak, O., Dolder, M., and Wallimann, T. (1996) Membrane-binding and lipid vesicle cross-linking kinetics of the mitochondrial creatine kinase octamer, *Biochemistry 35*, 15522−15528.
48. Kramer, S. D., Jakits-Deiser, C., and Wunderli-Allenspach, H. (1997) Free fatty acids cause pH-dependent changes in drug-lipid membrane interactions around physiological pH, *Pharm. Res. 14*, 827−832.
49. Seddon, J. M., Templer, R. H., Warrender, N. A., Huang, Z., Cevc, G., and Marsh, D. (1997) Phosphatidylcholine-fatty acid membranes: Effects of headgroup hydration on the phase behaviour and structural parameters of the gel and inverse hexagonal (H(II)) phases, *Biochim. Biophys. Acta 1327*, 131−147.
50. Templer, R. H., Seddon, J. M., and Duesing, P. M. (1998) Modeling the phase behaviour of the inverse hexagonal and inverse bicontinuous cubic phases in 2:1 fatty acid/phosphatidylcholine mixtures, *J. Phys. Chem. B 102*, 7262−7271.
51. Snapp, E. L., Hedge, R. S., Francolini, M., Lombardo, F., Colombo, S., Pedrazzini, E., Borgese, N., and Lippincott-Schwartz, J. (2003) Formation of stacked ER cisternae by low affinity protein interactions, *J. Cell Biol. 163*, 257−269.
52. Glabe, C. G. (1985) Interaction of the sperm adhesive protein, bindin, with phospholipid vesicles. I. Specific association of bindin with gel-phase phospholipid vesicles, *J. Cell Biol. 100*, 794−799.
53. Ulrich, A. S., Otter, M., Glabe, C. G., and Hoekstra, D. (1998) Membrane fusion is induced by a distinct peptide sequence of the sea urchin fertilization protein bindin, *J. Biol. Chem. 273*, 16748−16755.
54. Lambert, O., Cavusoglu, N., Gallay, J., Vincent, M., Rigaud, J. L., Henry, J.-P., and Ayala-Sanmartin, J. (2004) Novel organization and properties of annexin 2-membrane complexes, *J. Biol. Chem. 279*, 10872−10882.
55. Chattopadhyay, S., Sun, P., Wang, P., Abonyo, B., Cross, N. L., and Liu, L. (2003) Fusion of lamellar body with plasma membrane is driven by the dual action of annexin II tetramer and arachidonic acid, *J. Biol. Chem. 278*, 39675−39683.

56. Boggs, J. M., Yip, P. M., Rangaraj, G., and Jo, E. (1997) Effect of posttranslational modifications to myelin basic protein on its ability to aggregate acidic lipid vesicles, *Biochemistry 36*, 5065−5071.
57. MacMillan, S. V., Ishiyama, N., White, G. F., Palaniyar, N., Hallett, F. R., and Harauz, G. (2000) Myelin basic protein component C1 in increasing concentrations can elicit fusion, aggregation, and fragmentation of myelin-like membranes, *Eur. J. Cell Biol. 79*, 327−335.
58. Ruano, M. L. F., Miguel, E., Perez-Gil, J., and Casals, C. (1996) Comparison of lipid aggregation and self-aggregation activities of pulmonary surfactant-associated protein A, *Biochem. J. 313*, 683−689.
59. Williams, M. C., Hawgood, S., and Hamilton, R. L. (1991) Changes in lipid structure produced by surfactant proteins SP-A, SP-B, and SP-C, *Am. J. Respir. Cell Mol. Biol. 5*, 41−50.
60. Weber, T., Zemelman, B. V., McNew, J. A., Westermann, B., Gmachl, M., Parlati, F., Söllner, T. H., and Rothman, J. E. (1998) SNAREpins: Minimal Machinery for Membrane Fusion, *Cell 92*, 759−772.
61. Kent, C., and Carman, G. M. (1999) Interactions among pathways for phosphatidylcholine metabolism, CTP synthesis and secretion through the Golgi apparatus, *Trends Biochem. Sci. 24*, 146−150.
62. Huijbregts, R. T., Topalof, L., and Bankaitis, V. A. (2000) Lipid metabolism and regulation of membrane trafficking, *Traffic 1*, 195−202.
63. Howe, A. G., and McMaster, C. R. (2001) Regulation of vesicle trafficking, transcription, and meiosis: Lessons learned from yeast regarding the disparate biologies of phosphatidylcholine, *Biochim. Biophys. Acta 1534*, 65−77.
64. Cleves, A. E., McGee, T. P., Whitters, E. A., Champion, K., Aitken, J. R., Dowhan, W., Goebl, M., and Bankaitis, V. A. (1991) Mutations in the CDP-choline pathway for phospholipid biosynthesis bypass the requirement for an essential phospholipid transfer protein, *Cell 64*, 789−800.
65. Litvak, V., Dahan, N., Ramachandran, S., Sabanay, H., and Lev, S. (2005) Maintenance of the diacylglycerol level in the Golgi apparatus by the Nir2 protein is critical for Golgi secretory function, *Nat. Cell Biol. 7*, 225−234.
66. Amarilio, R., Ramachandran, S., Sabanay, H., and Lev, S. (2005) Differential regulation of endoplasmic reticulum structure through VAP−Nir protein interaction, *J. Biol. Chem. 280*, 5934−5944.
67. Feldman, D. A., and Weinhold, P. A. (1998) Cytidylyltransferase-binding protein is identical to transcytosis-associated protein (TAP/p115) and enhances the lipid activation of cytidylyltransferase, *J. Biol. Chem. 273*, 102−109.
68. Shorter, J., Beard, M. B., Seemann, J., Dirac-Svejstrup, A. B., and Warren, G. (2002) Sequential tethering of Golgins and catalysis of SNAREpin assembly by the vesicle-tethering protein p115, *J. Cell Biol. 157*, 45−62.

BI050679P